CHAPTER 5

Tailoring of ternary nanocomposite films of polyvinyl alcohol/$AgAlO_2$@reduced graphene oxide: An active material for flexible supercapacitors

CHAPTER 5

Tailoring of ternary nanocomposite films of poly(vinyl alcohol)/$AgAlO_2$@reduced graphene oxide: An active material for flexible supercapacitors

5.1. Abstract

Poly(vinyl alcohol) (PVA)/silver aluminium oxide ($AgAlO_2$)@reduced graphene oxide (RGO) nanocomposites (NCs) as flexible supercapacitor electrodes were fabricated via an eco-friendly and scalable solution casting approach. The crystallinity and morphological characteristics of the developed NCs were characterized by using X-ray diffraction (XRD), Raman spectroscopy, and scanning electron microscopy (SEM). The thermal properties were analyzed by thermal gravimetric analysis (TGA). The electrochemical performance of PVA/$AgAlO_2$@RGO NCs as a supercapacitor electrode material was investigated by cyclic Voltammetry (CV) studies. PVA/$AgAlO_2$@RGO NCs showed wide operating potential windows (1.2 V) which can greatly enhance their capacitive behavior. The highest specific capacitance obtained was 273.4 F g^{-1} in the case of 2 weight % $AgAlO_2$@RGO loaded PVA NC as compared to pristine PVA (6.04 F g^{-1}). These NCs exhibited superior performance with the energy density (13.8 $Whkg^{-1}$) and power density (150 W kg^{-1}) at 0.5 A g^{-1} respectively. PVA/$AgAlO_2$@RGO NCs exhibited the negligible equivalent series resistance and charge transfer resistance as an indication of excellent charge propagation at the interface between an electrolyte and an electrode. The NCs showed good capacity retention of 86.18 %, even after 1000 cycles. The NCs comprising of $AgAlO_2$ NPs exhibited better specific capacitance than reduced graphene oxide incorporated PVA NCs, thus constituting a new approach for fabricating supercapacitors electrodes.

5.2. Introduction

Recent research on solid-state devices used in supercapacitors has centred on mechanical flexibility, intending to achieve their high electrochemical efficiency while maintaining the remarkable trend of small, thin, lightweight, and flexible portable and wearable electronics, which exposes different new challenges for energy storage devices [1,2]. Supercapacitors are advanced energy storage systems that provide higher energy and power densities than conventional capacitors and batteries due to their advantages like long life cycle, durability, versatility, enhanced stability, and eco-friendliness [3]. They are useful for a variety of purposes such as electric vehicles, distributed sensor networks, mobile electronic devices, etc, [4,5]. Such devices have attracted research interest around the world and this has resulted in several research projects in the desired field. The mechanism of charge storage in supercapacitors is broadly categorized into two categories: (i) electrochemical double-layer capacitor (EDLC), where capacitance is caused by charge accumulation at the interface between the electrode and the electrolyte used, and (ii) pseudo capacitor, where reversible faradaic reactions on the surface of an electrode cause the capacitance [6]. Since the functioning of a supercapacitor is affected by the features of electrode materials, advanced electrode materials have to be developed and the efficiency of presently available materials has to be improved. However, since the development of the supercapacitor, researchers have continued to look for excellent electrode material. Several carbon-containing materials and their combinations have been studied for electrode fabrication in order to achieve high-efficiency supercapacitors. The widely researched community includes graphene/transition metal oxide nanocomposites (NCs), transition metal oxide/carbon NCs, polymer nanofibers incorporated with graphene oxide (GO), polymer/reduced graphene oxide

(RGO)/metal oxide NCs and so on, [7-10]. Kalim Deshmukh et al fabricated a ternary NC by simple solution casting, poly (vinyl alcohol) (PVA)/V_2O_5/GO, a flexible electrode with different GO content (0 – 2.5 wt %), and it was noticed that NC with GO content 2.5 wt% possessed exceptional properties. The Dielectric constant of NC with GO content of 2.5 wt % was 5610.7 at 50 Hz [11]. Saira Ishaq et al have prepared three-phase PVA/ graphene/titania NC films and obtained a dielectric constant of 330 at 20 Hz, which is 36 times higher than pure PVA [12]. However, some concerns such as capacitance value, stability, and negative environmental effect restrict the use of certain combinations.

Because of structural conformation, shrinkage, cracks, and other factors, nano metal oxides are commonly used as electrode materials, which have some demerits due to solubility and processability issues, poor mechanical properties, and reduced environmental resistivity [13,14]. Besides these drawbacks, nano metal oxides offer some benefits such as excellent permanence, tunable electrical properties, good electrochemical property, better surface area, and potential of compounding with polymers, to be used as a suitable material in electrode applications [15-17]. The transition metal oxides are of great interest as pseudocapacitor electrodes in developing advanced high-efficiency energy storage devices because of their excellent productivity or energy output as compared to EDLC materials [18]. According to scientific studies, metal oxides need additional materials with good properties to address their main drawbacks. Poly(vinyl alcohol) has a high processibility and water solubility, and it can be used as a matrix for other products [19]. Because of its low mechanical and thermal properties, PVA allows other materials to be easily reinforced into its structure. But apart from polymers and transition metals, an allotrope of carbon such as graphene has gained tremendous

attention in the research field. The latest research has shown that adding graphene derivatives to aqueous polymer solutions will enhance the properties of the NCs [20]. Structurally, RGO) is a monolayer sp^2 hybridized carbon atoms in a hexagonal network derived from graphene (a one-atom-thick layer of graphite). Thus, RGO is widely used in the areas such as supercapacitors [21,22], solar cells [23,24], fuel cell [25,26], sensors [27,28] etc. Kandhol Geeta, et al [29] reported that rGO infusion into the PVA matrix improves its mechanical strength. In another work, the researchers fabricated rGO-PVA films to achieve the benefit of the synergy of a combination of desirable attributes of both components [30]. Sharma et al and Park et al demonstrated a significant improvement in the mechanical properties by incorporating rGO into the PVA matrix [31,32]. Zhang et al [33] investigated the good bonding between PVA and GO because of the high specific surface area of GO nanoparticles. According to studies, nanostructured electrode materials are required because of their ability to offer greater charge-discharge rates [34]. The surface area, structure, morphology, and conductivity of the electrode material had a major impact on supercapacitor output [35,36]. So, the electrochemical properties may change based on the nature of electrode-electrolyte interaction. PVA is accepted as the best among all polymers because of its high adhesion property and –OH side groups allow electron mobility [37,38]. The uniform dispersion of rGO and silver aluminium oxide ($AgAlO_2$) nanoparticles (NPs) in the PVA matrix is because of the active hydroxyl groups in the polymer, which leads to hydrogen bond formation between the components present in the NC [30]. Constructive reinforcement of $AgAlO_2$@rGO in the PVA matrix would result in an efficient NC for energy storage.

This work also provides a comparison of specific capacitance values obtained by different formulations of PVA with $AgAlO_2$ decorated rGO ($AgAlO_2$@rGO),

which is prepared via facile solution casting technique to be used as supercapacitor electrodes. The NCs prepared with different concentration of $AgAlO_2$@rGO Hybrid nanoparicals were designated as 0.5 PNC, 1PNC, 2PNC & 4PNC for 0.5, 1, 2 & 4wt% of $AgAlO_2$@rGO respctively. The super-capacitive behavior of PVA/$AgAlO_2$@rGO NCs has been studied by using cyclic voltammetry (CV) in 1 M Na_2SO_4 electrolyte. The electrochemical analysis results indicate that the metal oxide decorated rGO greatly affects the redox reaction activity. This investigation provides a facile synthetic strategy to achieve atomically, 2D nanosheets intercalation inside polymer chain and will undoubtedly uphold the understanding of the effects of the decorated hybrid nanoparticles on electrochemical storage.

5.3. Results and discussion

Structural and Morphological characterization of flexible PNC films

A scanning electron microscope (SEM) has been utilized to analyze the structural and morphological effects of $AgAlO_2$@rGO inside the PVA matrix. Figures 5.1(a-c) present the SEM images of rGO, $AgAlO_2$, and $AgAlO_2$@rGO respectively at better resolutions. From the SEM image Figure, 5.1(a) is noticed that well reduced dispersed layers of rGO, in Figure 5.1(b) well depicts that formation of spherical like the structure of as-synthesized $AgAlO_2$ and the inset figure shows the magnified area of NPs, that depict the spherical structured of NPs. EDS spectra from Figures 5.1(d-f) also supports the formation of rGO, $AgAlO_2$, and the presence of NPs and rGO in $AgAlO_2$@rGO hybrid filler. Elemental quantification also clearly depicts the atomic and wt% of individual components present in the hybrid filler were tabulated in table 5.1. Figure 5.1(c) shows the well-decorated NPs on reduced graphene oxide layers and they are well dispersed. The interactions of oxygen-containing functional groups present on the surface of rGO layers with metal oxides prevent aggregation [40].

FTIR data also supports the very good interaction between the oxygen functional groups present in the rGO and oxygen present in the metal oxide NPs showed in Figure 5.6(a). As per the previous reports, these structures offer more active sites for excellent electrochemical performance leading to effective electron transport during cycling [41].

After fabrication of PVA/$AgAlO_2$@rGO PNCs, the dispersion of nanofillers inside the PVA matrix was studied using SEM. Figure 5.2(a-e) shows the SEM images of pure PVA, 0.5 PNC, 1PNC, 2PNC, and 4PNC. As from the images, PNCs show well-dispersed nanofillers up to 2 wt% $AgAlO_2$ loaded PNCs, after 4 wt% loading PNCs shows agglomerations of NPs. The PNCs show the increase in roughness with the increase in the concentration of nanofillers inside the PVA matrix [42], 2 PNC shows well dispersion and uniform roughness over the film which is further, studied using DM surface analysis. Figure 5.2(e) depicts the EDS mapping image of 2PNC, which represents the atomic wt% of elements present and dispersion of $AgAlO_2$@rGO inside the PVA matrix.

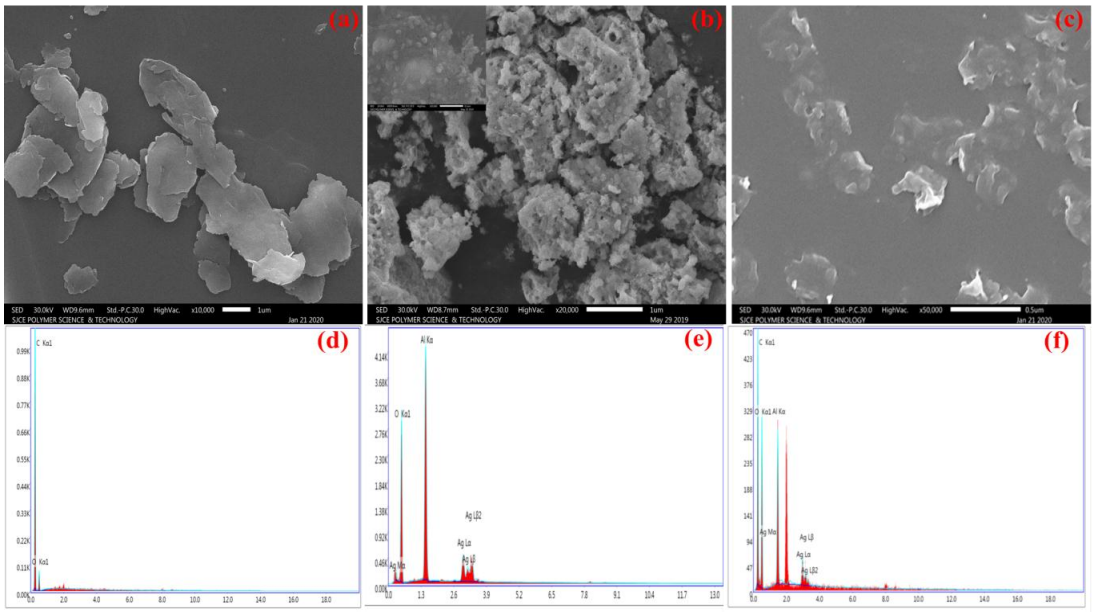

Figure 5.1. SEM photomicrographs of (a) rGO, (b) $AgAlO_2$, (c) $AgAlO_2$@rGO, and EDS spectra of (d) rGO, (e) $AgAlO_2$, and (f) $AgAlO_2$@rGO

Table 5.1. EDS results of elemental quantification of rGO, $AgAlO_2$ and 2 wt% $AgAlO_2$@ rGO

eZAF Smart Quant Results			
Sample	**Element**	**Weight %**	**Atomic %**
rGO	C K	81	85.03
	O K	19	14.97
$AgAlO_2$	Ag L	12.64	2.53
	Al K	36.90	29.48
	O K	50.46	67.99
$AgAlO_2$@ rGO	C K	49.35	60.08
	O K	40.48	35.45
	Al K	7.71	4.14
	Ag L	2.46	0.33

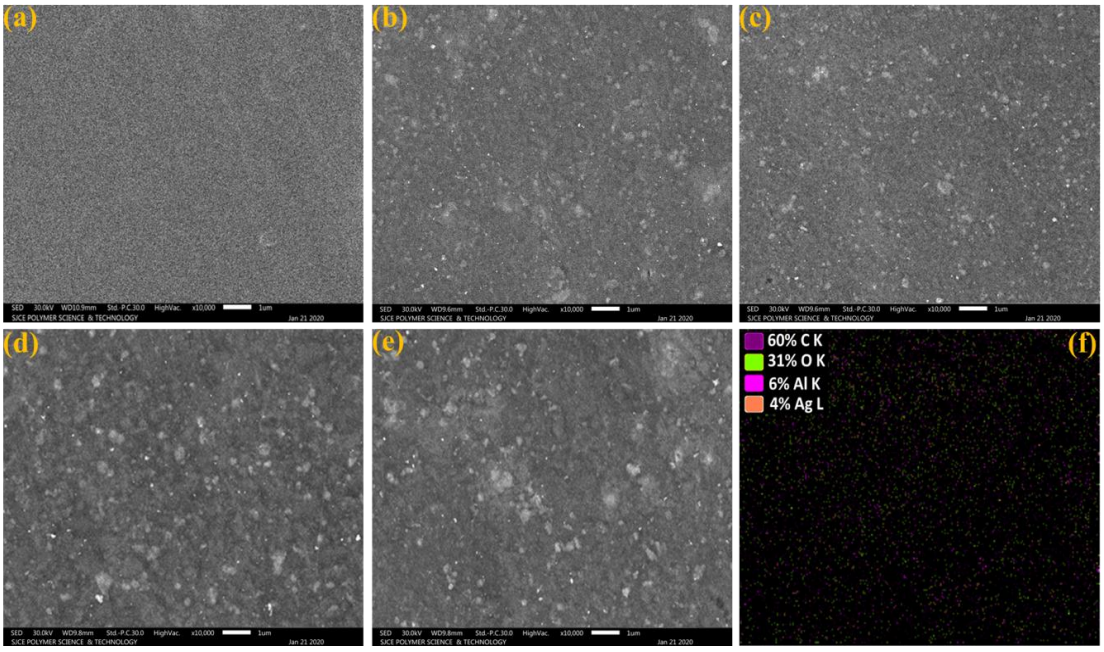

Figure 5.2. SEM images of (a) pure PVA, (b) 0.5 PNC (c) 1PNC, (d) 2PNC, (e) 4PNC and (f) EDS mapping image of 2 PNC

The effect of varying amounts of $AgAlO_2$@rGO on the surface roughness of the PVA/$AgAlO_2$@rGO NCs was further investigated and compared with pristine

PVA by using DM surface images Figure 5.3(a-c) at 300 µm x 300 µm scan area. The roughness values of surfaces of the as-prepared NCs were compared with pristine PVA. As presented in Figure 5.3(c) the overall gradual increasing trend in the surface roughness as compared to pristine PVA film could be due to increased $AgAlO_2$ content in the polymer matrix. The roughness of the NCs increased uniformly over the surface, indicates the good dispersion of NPs in the PVA matrix.

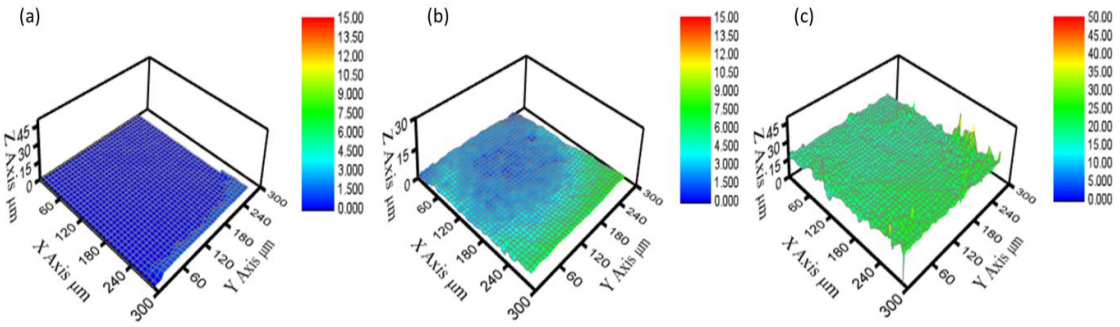

Figure 5.3. DM surface images of the (a) pristine PVA, (b) 0.5 PNC, and (c) 2PNC

Comparative crystal structure characterization of the rGO, $AgAlO_2$, $AgAlO_2$@rGO, and their NCs have been performed by XRD, and obtained profiles are shown in Figure 5.4a. The signature peak of rGO is noticed at 2θ of ~25° (002). It concludes GO complete reduction to form rGO with a d spacing of 0.355 nm. However, this peak is broad and confirms the destruction of regular stacks of graphene layers, prepared via the hydrothermal method. In the XRD spectrum of $AgAlO_2$@rGO composite, the diffraction peaks obtained at 2θ of 25°, 38.0°, 44.3°, 64.5°, and 77.4° correspond to lattice planes of (002), (111), (200), (220), and (331), respectively. The indexed peaks represent a face centered cubic lattice phase for $AgAlO_2$, which are in good agreement with the data published elsewhere [39]. The crystalline peaks of metal oxide NPs were not disturbed in the XRD pattern of $AgAlO_2$@rGO indicate there is no chemical change in the NPs. There are no extra peaks found in the XRD spectrum of hybrid NPs confirming the high purity of

materials and also reveals that the $AgAlO_2$ NPs have been homogeneously dispersed on the surface of the rGO layers [43]. To further confirm the phase purity of prepared NPs, EDS analysis was carried out. The EDS result exhibits the phase purity of $AgAlO_2$@rGO NCs with desired elemental composition as C, O, Ag, and Al with no other impurities. This is supported by the XRD result and quantification data provided in Table 5.1. Figure 5.4(b) depicts the XRD spectra of pristine PVA and the PVA/$AgAlO_2$@rGO NCs. Pure PVA shows a semicrystalline diffraction peak at 2θ of 19.6°. A slight shifting of peak position appeared at 2θ of 19.3° is noticed with change in compositions of NCs. There are no prominent peaks appeared for NPs, it may be due to the overlapping of NPs by the polymer chains, also indicating the uniform dispersion and reinforcement of NPs in the polymer matrix. The minor peak at around 2θ of 38° for NPs exhibits in the XRD pattern of 4 PNC. As can be observed the intensity of the semicrystalline characteristic peak of PVA is decreased and the peak becomes broader it may be due to intercalation between NPs and polymer chains, which may lead to loss of intermolecular hydrogen bonding which reduces the semicrystalline nature of PVA.

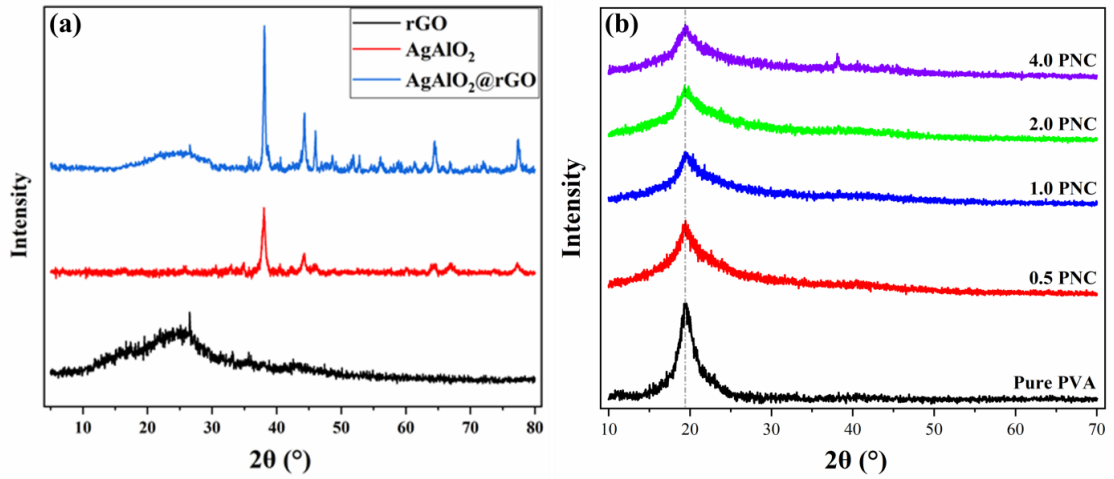

Figure 5.4. XRD patterns of (a) rGO, $AgAlO_2$, $AgAlO_2$@rGO and (b) pure PVA, 0.5 PNC, 1 PNC, 2 PNC and 4 PNC nanocomposites

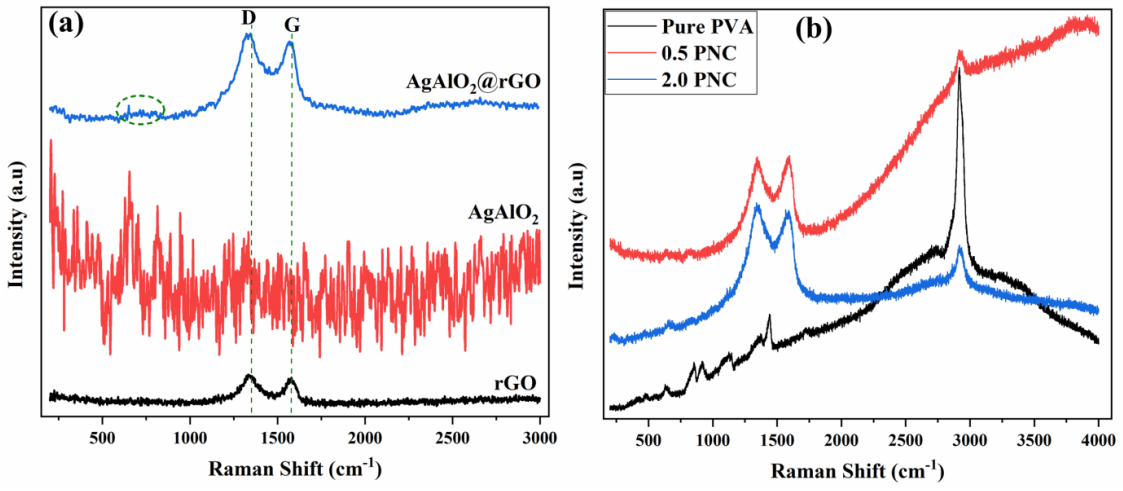

Figure 5.5. FT-Raman spectra of (a) rGO, $AgAlO_2$, $AgAlO_2$@rGO and (b) Pristine PVA and pure PVA, 0.5 PNC, and 2 PNC nanocomposites

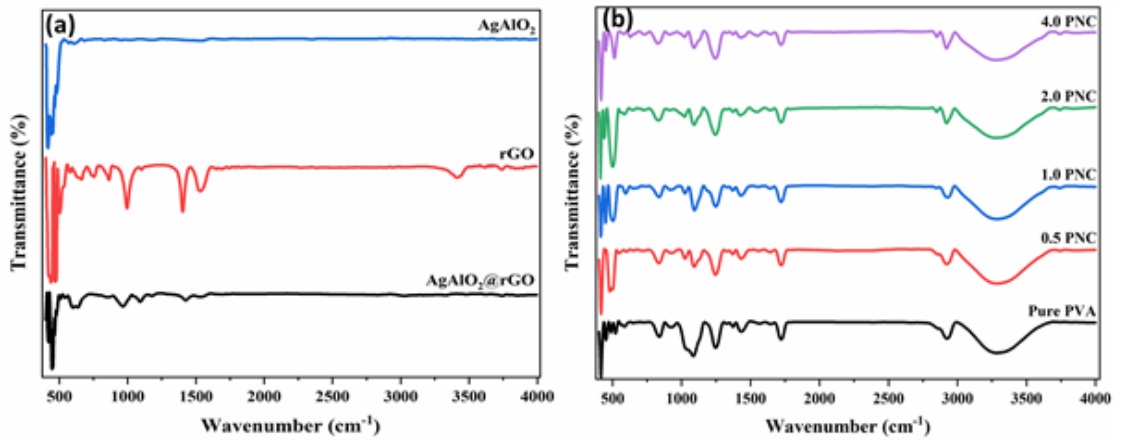

Figure 5.6. FTIR spectra of (a) $AgAlO_2$, rGO and $AgAlO_2$@rGO and (b) pure PVA and $AgAlO_2$@rGO / PVA composites with different wt% of NPs decorated on rGO loaded PVA composites

The interactions between graphene layers and NPs, and polymer chains, and hybrid NPs, $AgAlO_2$@rGO were established by FT-Raman spectral studies. Figure 5.5(a) displayed the Raman spectra of the as-synthesized rGO, $AgAlO_2$, and $AgAlO_2$@rGO samples. The peaks corresponding to D and G - bands of rGO were appeared at 1345 and 1580 cm^{-1}, respectively. The D band peak shows a reduction in the symmetry indicating the defects in the layers. The G-band corresponds to

suppression in-plane E_{2g} optical mode at the center of graphitic carbon's Brillouin zone [44]. The peak observed at 656, 810, and 1184 cm^{-1} for NPs (red curve) are attributed to the metal-oxygen bonds of $AgAlO_2$ [45]. After the introduction of NPs inside graphene oxide layers, the D and G-bands are red-shifted to 1333 and 1571 cm^{-1} (blue curve) respectively. The intensity ratio (I_D/I_G) value for rGO was 1.18, whereas for $AgAlO_2$@rGO I_D/I_G value was increased to 1.23. These changes confirm the effective hydrothermal reduction of GO and $AgAlO_2$ was decorated on the graphene layer by breaking of sp^2 carbon structure in the graphitic structures of rGO [43].

The Raman spectra of PVA/$AgAlO_2$@rGO NC films are depicted in Figure 5.5(b). For 0.5 PNC, a slightly weak D and G bands have appeared at 1350, and 1580 cm^{-1} respectively. For PNC with 2 wt% $AgAlO_2$ NPs, the D band was observed at 1345 cm^{-1} with slightly higher intensity than the G band. The enhancement of the intensity of the D band suggests a good interaction between polymer chains and graphene layers. This is well correlated with FTIR spectra of PNCs Figure 5.6 (b), which shows the decrease in intensity of characteristic peaks after incorporating $AgAlO_2$@rGO. This indicates the interaction of nanofillers and polymer chains. The bands at 656 cm^{-1} and 810 cm^{-1} in polymer NCs are due to NPs. Thus, the existence of $AgAlO_2$@rGO NPs in the PVA matrix was confirmed by Raman spectra.

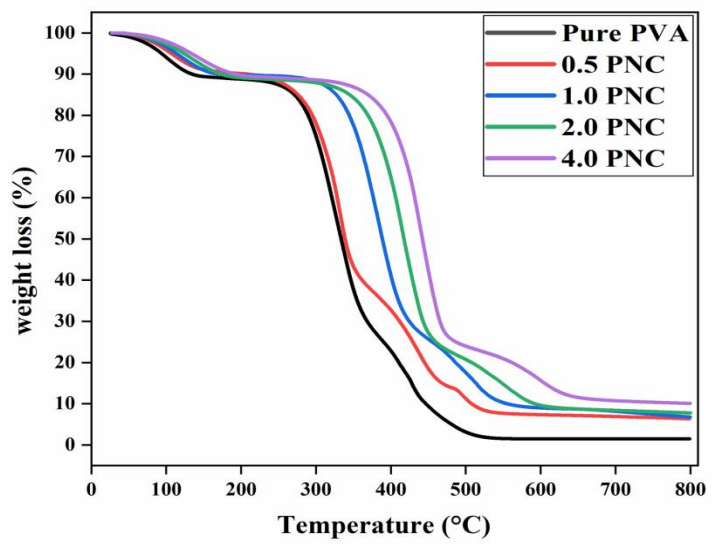

Figure 5.7. TGA thermograms of PVA, 0.5 PNC, 1 PNC, 2 PNC, and 4 PNC

TGA studies have been carried out to investigate the thermal behaviour of $AgAlO_2$@rGO incorporated PVA NCs. The thermograms of PVA and PVA/$AgAlO_2$@rGO NCs are depicted in Figure 5.7. The thermogram indicates that the slight loss of weight at below 200 °C for PVA and PVA/$AgAlO_2$@rGO NC and is because of moisture content. For PVA the highest weight loss observed at the temperature between 275 - 400 °C, which is due to break down of functional groups and main chains of PVA, then finally residual carbon also completely degrade at 515 °C [46]. However, it is clear from the thermogram of PVA/$AgAlO_2$@rGO, it is more thermally resistant than bare PVA. The onset of thermal degradation of PVA NCs containing 0.5, 1, 2, and 4 wt % of $AgAlO_2$@rGO NPs was at 278, 350, 380, and 405 °C respectively. The residual percentage was gradually increased from 4.5 % of PVA to 13% for 4 PNC. It is due to the intercalation of $AgAlO_2$@rGO in between polymer chains [47].

Electrochemical studies of fabricated PNC films for supercapacitors

The shape of the CV curve (Figure 5.8 (a)) can be attributed to both EDLC and pseudocapacitance behaviours contributed by rGO and $AgAlO_2$ respectively. CV curves of PVA/$AgAlO_2$@rGO NC electrode maintain a similar shape but with increasing NPs content up to 2 PNC the redox peak has clearly appeared. In the case of 4 PNC shows anomalous behaviour, even though higher content of NPs loading, the redox peaks were absent, it may be due to agglomerations of NPs. The role of $AgAlO_2$@rGO in improving the electrochemical properties of NCs has thus been discovered. The importance of NPs over rGO layers for the mobility of electrons and large specific surface area, enhancing the material's basic capacitance, also has been demonstrated [48]. All these explain the capability of rGO based NCs as electrode materials for supercapacitors. Specific capacitance (C_{sp}), energy density (*E*), and power density (*P*) of PVA/$AgAlO_2$@rGO NCs have been evaluated by obtaining galvanostatic charge-discharge curves from the eqns. (1)–(3), respectively.

$$C_{sp} = \frac{I\Delta t}{m\Delta V} \tag{1}$$

$$E = \frac{\Delta V^2}{2 \times 3600} Cs \tag{2}$$

$$P = \frac{E \times 3600}{\Delta t} \tag{3}$$

Where, C_{sp} (F g^{-1}) denotes the electrode's unique capacitance; I(A) represents the discharge current; t (s) is the discharge duration; m (g) indicates the active material's mass, and V (V) indicates the potential window. Specific capacitance values of 6.04 F g^{-1} and 273.4 F g^{-1} were achieved for PVA and 2 PNC respectively. The reason for the greater current value of 2 PNC is because of the redox peak which

is attributed to the pseudocapacitive behaviour of $AgAlO_2$. The presence of rGO increased the overall real capacitance of PVA/$AgAlO_2$@rGO NCs by contributing to electrical double layer capacitance.

Figure 5.8(b) depicts galvanostatic charge-discharge (GCD) curves for PVA and PVA/$AgAlO_2$@rGO exhibiting consistent results with those of CV graphs of NCs. It is observed that the discharge time of PVA/$AgAlO_2$@rGO is far higher than that of pristine PVA. The enhanced electrochemical efficiency of PVA after incorporation of $AgAlO_2$@rGO can be described by considering the electrically conductive nature of rGO and $AgAlO_2$ which, leads to efficient diffusion of ions into the electroactive electrode material as well as to the synergistic effect of the 3 components within ternary PVA/$AgAlO_2$@rGO NCs [49]. GCD profiles of PVA/$AgAlO_2$@rGO at dissimilar current densities like 0.5, 1, 2, 5, and 10 Ag^{-1} are depicted in Fig. 8(a). At all current densities, all CD curves are extremely similar, showing that the electrode material has ideal capacitive behaviour. The discharge time of the 2PNC electrode is the maximum of all the synthesized electrodes, showing that the electrode material exhibits higher conductivity, lower internal resistance, and strong rate capability in the investigated electrolyte, 1 M Na_2SO_4.

As with an improved current density, restricted diffusion of charges results in moderate specific capacity; Figure 5.9 (b) depicts how efficiently 2PNC can maintain C_{sp}, even with raising current density. The specific power and specific energy for 2PNC under different current density values of 0.5 - 10 A g^{-1} were calculated and the inset of the Ragon plot for 2PNC is shown in Figure 5.9 (b). The energy density has to be increased without any loss of power supply to produce highly advanced supercapacitors for practical usage. To enhance the energy density of flexible supercapacitors, improved C_{sp} with a broad operating ideal potential window is essential. At 0.5 Ag^{-1} specific power and specific energy of 2.0 PNC are 150 W kg^{-1}

and 13.8 W h kg^{-1} respectively. This is increased to 3000 W kg^{-1} at 10 A g^{-1}, while specific energy value is retained as 8.8 W h kg^{-1} at 10 A g^{-1}. An increase in specific energy from pristine PVA to PVA/$AgAlO_2$@rGO is because of an increase in conductivity, due to the incorporation of $AgAlO_2$@rGO NPs. Cyclic stability was also studied for as- fabricated 2 PNC film for 1000 charge/discharge cycles under current density value 0.5 A g^{-1} and PNCs presents better stability retention of 81%. After 1000 cycles, there was no discernible decrease in capacitance, indicating the high cycle stability as well as the high extent of reversibility in the repeated charge-discharge analysis [50].

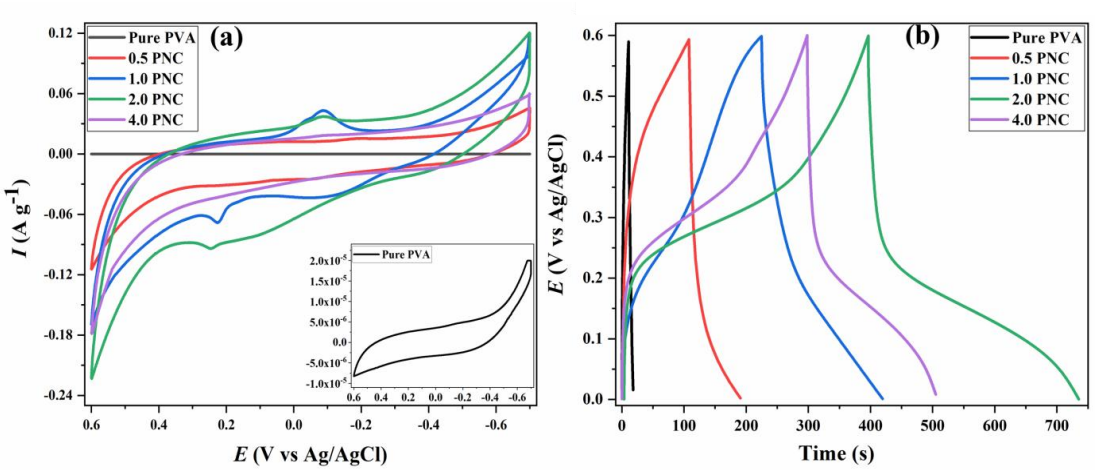

Figure 5.8. (a) CV curves of pure PVA, 0.5 PNC, 1 PNC, 2 PNC and 4 PNC under scan rate 50 mV s^{-1} and (b) GCD profiles for neat PVA and 0.5 PNC, 1 PNC, 2 PNC, and 4 PNC at a current density value of 0.5 A g^{-1}.

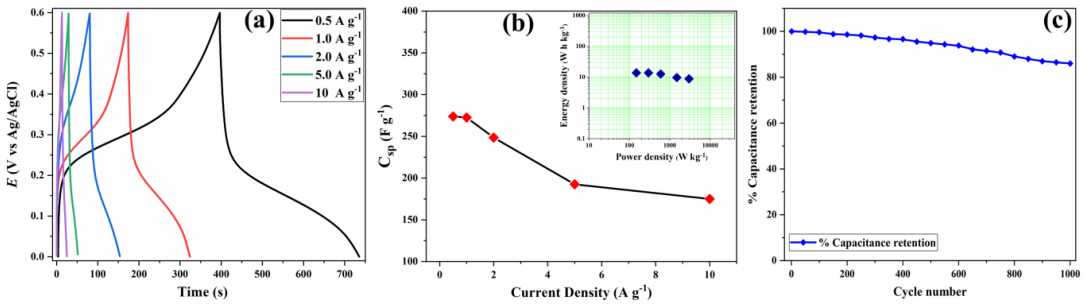

Figure 5.9. (a) GCD curves, (b) Specific capacitance with inset of Regone plots of the 2 PNC at 0.5, 1, 2, 5, and 10 A g^{-1} current densities, and (c) The cyclic stability of the 2 PNC film for 1000 charge/discharge cycles under current density value of 0.5 A g^{-1}.

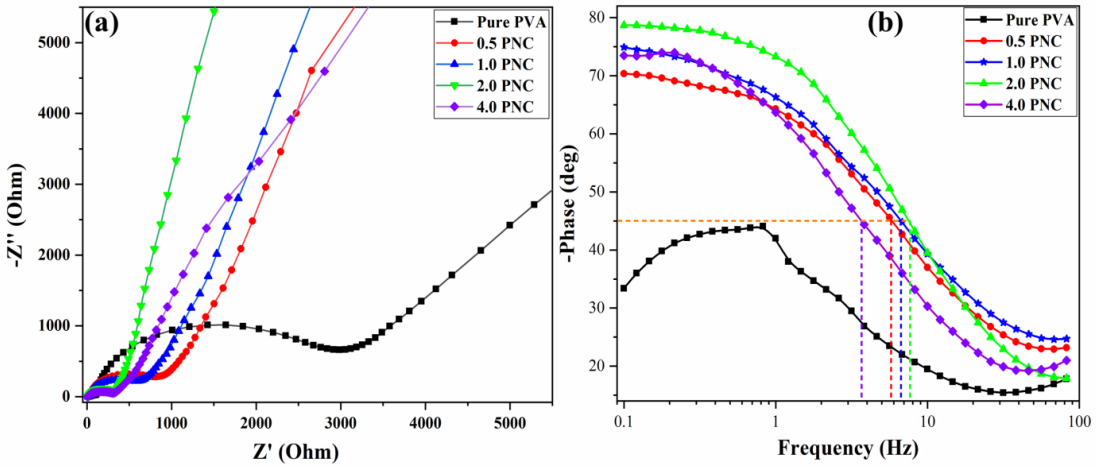

Figure 5.10. (a) Nyquist plots and (b) Bode plots for pure PVA and 0.5, 1, 2, and 4 PNC films.

In 1 M Na_2SO_4, electrochemical impedance spectroscopy (EIS) was carried out by using a 3-electrode device at a 5 mV exciting potential in the frequency range 0.01–100 kHz, with the Nyquist plot shown in Figure 5.10 (a). The Nyquist plot tells that PVA/$AgAlO_2$@rGO composites show small semicircles at a region of greater frequency, the semicircle diameter represents the interfacial charge transfer resistance (*R*ct), while the straight line in the greater frequency zone reveals Warburg resistance (ion diffusion resistance). 2 PNC exhibits very small equivalent series resistance (ESR) of 9 Ω whereas PVA shows higher resistance of 104 Ω. This ESR was derived from the first x-intercept of plots [51,52]. However, at lower frequency region PVA/$AgAlO_2$@rGO NCs have greater slopes when compared with the slope of PVA, which indicates that NCs have much greater capacitance performance than pristine PVA, which is consistent with CV and GCD profile results. Figure 5.10 (b) is Bode phase plot for pure PVA and PVA/$AgAlO_2$@rGO NCs. The 0.5, 1, 2, and 4 PNCs demonstrate that at the region of lower frequency, the phase shift will be as, −70°, −74°, −78°, and −73° respectively, confirming that the material functions as a capacitor, with good diffusion process[53]. The phase angle attains −45° at capacitor response frequency of 7.6 Hz for 2 PNC, which is significantly higher than rGO (1.7 Hz) [54].

The electrochemical performance of the fabricated ternary PVA/$AgAlO_2$@rGO electrodes is compared with the electrochemical performance of previously recorded electrodes in Table 5.2. When our findings are compared to previous literature findings, it becomes clear that ternary PVA/$AgAlO_2$@rGO electrodes provide superior electrochemical efficiency. The incorporation of $AgAlO_2$@rGO NPs as a hybrid component in the PVA matrix, which enhances electrochemical efficiency due to its redox behaviour, is suggested as a possible explanation for this improvement.

Table 5.2. The specific capacitance of PVA/$AgAlO_2$@rGO nanocomposite when compared with that of other rGO based composites

Materials	Electrolyte	Specific Capacitance ($F\ g^{-1}$)	Energy Density (W h/kg)	Power Density (W/kg)	Potential window (V)	Reference
PVA-RGO PVA-GO	1 M H_2SO_4	190 13			0.8	[55]
PVA-GO/PEDOT	1 M KCl	224.2	9.58	304.3	1.0	[56]
PVA-GO-MnO_2/PEDOT	1 M KCl	144.6	9.60	243.7	1.0	[57]
PANI/γ-Al_2O_3	0.5 M H_2SO_4	292			1.1	[58]
RGO/PIn/γ-Al_2O_3	1.0 M $HClO_4$	302	10	3880	0.9	[59]
CuO/rGO	1.0 M Na_2SO_4	80			1.2	[60]
PANI/rGO/Ag_2O	1 M H_2SO_4	255.7			1.0	[61]
PVA/SF-SWNT	0.1 M KCl	26.4			0.9	[62]
RGO-PVA	0.5 M KCl	198			1.0	[63]
PANI/PVA/GO	1 M H_2SO_4	438.8			1.2	[64]
2 PNC	1 M Na_2SO_4	273.4	13.7	150	0.6	This Work

The specific capacitance of PVA/$AgAlO_2$@rGO is better than previously reported PVA/GO, and PVA/RGO NC electrode [55] which is due to better conductivity of rGO than GO and high ion exchange property of $AgAlO_2$, hence it is one of the best candidates to improve electrochemical performance. Elmira et al [59] have reported on RGO/PIn/γ-Al_2O_3 electrodes supply better gravimetric capacitance

than fabricated NCs because, in the preparation of this composite, the electrochemical deposition method was used to disperse it effectively on gold plate and polymer matrix. Also because of the existence of all three better-conducting constituents, each of them is effectively contributed to enhancing the electrochemical performances of the resultant composite. In addition, electrolyte reported in the literature is dissimilar from this investigation. Aleena et al reported [64] better specific capacitance of PANI/PVA/GO electrodes compared to our fabricated ternary composites, which can be due to nanofiber morphology of active material, nanofiber were obtained via electrospinning process, and the studies conducted using CV at 100 mV S^{-1}. Usually, at a high scan rate, gravimetric capacitance is more and which reduces based on the decreasing scan rate. The specific capacitances of PANI/rGO/Ag_2O [61] and PANI/γ-Al_2O_3 [58] electrode previously reported elsewhere are almost equal to that of as-synthesized PVA/$AgAlO_2$@rGO electrodes. It is because of the existence of better-conducting components in the system.

5.4. Summary

In summary, we have successfully demonstrated the facile fabrication of $AgAlO_2$@rGO and PVA/$AgAlO_2$@rGO NCs via a simple solution casting technique. The phase constituents and morphological features of $AgAlO_2$@rGO and PVA/$AgAlO_2$@rGO are confirmed by XRD and SEM analysis respectively. SEM images of $AgAlO_2$@rGO and PVA/$AgAlO_2$@rGO NCs indicate the homogeneous dispersion of NPs in the polymer matrix. The electrochemical performance of 2 PNC electrodes achieves the highest specific capacitance of 273.4 F g^{-1} when related to PVA (6.04 F g^{-1}) and it is the optimized formulation. This research investigation revealed the greatest advantage of $AgAlO_2$, rGO, and $AgAlO_2$@rGO on specific capacitance results of the PVA NCs. It has been concluded that a trace amount of rGO

and $AgAlO_2$ can lead to significant variation in the electrochemical properties of flexible NC films. The overall conclusion is as prepared ternary PVA/$AgAlO_2$@rGO NCs are a promising candidate to be used as an electrode material for supercapacitors with effective electrochemical performance.

5.5. References

1. Rogers, John A., Takao Someya, and Yonggang Huang. "Materials and mechanics for stretchable electronics." science 327.5973 (2010): 1603-1607.
2. Nyström G, Mihranyan A, Strømme M. Toward flexible polymer and paper-based energy storage devices. Advanced Materials. 2011, 1;23(33):3751-69.
3. Gonçalves LM, de Zea Bermudez V, Ribeiro HA, Mendes AM. Dye-sensitized solar cells: A safe bet for the future. Energy & Environmental Science. 2008; 1(6):655-67.
4. Simon P, Gogotsi Y. Review: materials for electrochemical capacitors. Nature Materials. 2008; 7:845-54.
5. Khairy, Mohamed, and Sherif A. El-Safty. "Hemoproteins–nickel foam hybrids as effective supercapacitors." Chemical Communications 50.11 (2014): 1356-1358.
6. Guo, Bingkun, et al. "Soft-templated mesoporous carbon-carbon nanotube composites for high performance lithium-ion batteries." Advanced materials 23.40 (2011): 4661-4666.
7. He F, Lau S, Chan HL, Fan J. High dielectric permittivity and low percolation threshold in nanocomposites based on poly (vinylidene fluoride) and exfoliated graphite nanoplates. Advanced Materials. 2009, 9;21(6):710-5.
8. Bao, Qiaoliang, et al. "Graphene–polymer nanofiber membrane for ultrafast photonics." Advanced functional materials 20.5 (2010): 782-791.
9. Bao, Chenlu, et al. "Poly (vinyl alcohol) nanocomposites based on graphene and graphite oxide: a comparative investigation of property and mechanism." Journal of Materials Chemistry 21.36 (2011): 13942-13950.

10. Wang, Ning, et al. "Graphene–poly (vinyl alcohol) composites: Fabrication, adsorption and electrochemical properties." Applied Surface Science 314 (2014): 815-821.
11. Deshmukh, Kalim, et al. "Synergistic effect of vanadium pentoxide and graphene oxide in poly(vinyl alcohol) for energy storage application." European Polymer Journal 76 (2016): 14-27.
12. Ishaq, Saira, et al. "Dielectric and impedance spectroscopic studies of three phase graphene/titania/poly (vinyl alcohol) nanocomposite films." Results in Physics 11 (2018): 540-548.
13. An, Cuihua, et al. "Metal oxide-based supercapacitors: progress and prospectives." Nanoscale Advances 1.12 (2019): 4644-4658.
14. Jiang J, Li Y, Liu J, Huang X, Yuan C, Lou XW. Recent advances in metal oxide-based electrode architecture design for electrochemical energy storage. Advanced Materials. 2012, 2; 24(38):5166-80.
15. Fan Z, Huang X, Tan C, Zhang H. Thin metal nanostructures: synthesis, properties and applications. Chemical Science. 2015;6(1):95-111.
16. Chang X, Zang L, Liu S, Wang M, Guo H, Wang C, Wang Y. In situ construction of yolk–shell zinc cobaltite with uniform carbon doping for high performance asymmetric supercapacitors. Journal of Materials Chemistry A. 2018; 6(19):9109-15.
17. Trasatti, Sergio, and Giovanni Buzzanca. "Ruthenium dioxide: a new interesting electrode material. Solid state structure and electrochemical behaviour." Journal of electroanalytical chemistry and interfacial electrochemistry 29.2 (1971): A1-A5.
18. Zhi, Mingjia, et al. "Nanostructured carbon–metal oxide composite electrodes for supercapacitors: a review." Nanoscale 5.1 (2013): 72-88.

19. Subramani NK, Kasargod Nagaraj S, Shivanna S, Siddaramaiah. Highly flexible and visibly transparent poly (vinyl alcohol)/calcium zincate nanocomposite films for UVA shielding applications as assessed by novel ultraviolet photon induced fluorescence quenching. Macromolecules. 2016, 12; 49(7):2791-801.
20. Sun, Jingjing, et al. "Hydrated vanadium pentoxide/reduced graphene oxide-poly(vinyl alcohol) (V2O5· nH2O/rGO-PVA) film as a binder-free electrode for solid-state Zn-ion batteries." Journal of Colloid and Interface Science 587 (2021): 845-854.
21. Singh, Arvind, Saurav K. Ojha, and Animesh K. Ojha. "Facile synthesis of porous nanostructures of NiCo2O4 grown on rGO sheet for high performance supercapacitors." Synthetic Metals 259 (2020): 116215.
22. Jadhav, Sarika, et al. "Manganese dioxide/reduced graphene oxide composite an electrode material for high-performance solid state supercapacitor." Electrochimica Acta 299 (2019): 34-44.
23. Cai, Haopeng, et al. "Nanostructured composites of one-dimensional TiO2 and reduced graphene oxide for efficient dye-sensitized solar cells." Journal of Alloys and Compounds 697 (2017): 132-137.
24. Wang, Liqun, et al. "A reduced graphene oxide interface layer for improved power conversion efficiency of aqueous quantum dots sensitized solar cells." International Journal of Hydrogen Energy 44.1 (2019): 128-135.
25. Farooqui UR, Ahmad AL, Hamid NA. Graphene oxide: a promising membrane material for fuel cells. Renewable and Sustainable Energy Reviews. 2018, 1;82:714-33.
26. Bayer T, Selyanchyn R, Fujikawa S, Sasaki K, Lyth SM. Spray-painted graphene oxide membrane fuel cells. Journal of Membrane Science. 2017, 1; 541:347-57.

27. Xu, Minxuan, et al. "Highly stretchable strain sensors with reduced graphene oxide sensing liquids for wearable electronics." Nanoscale 10.11 (2018): 5264-5271.
28. Sharma, Neeru, et al. "Synthesis and characterization of graphene oxide (GO) and reduced graphene oxide (rGO) for gas sensing application." Macromolecular Symposia. Vol. 376. No. 1. 2017.
29. Kandhol G, Wadhwa H, Chand S, Mahendia S, Kumar S. Study of dielectric relaxation behavior of composites of Poly(vinyl alcohol)(PVA) and Reduced graphene oxide (RGO). Vacuum. 2019, 1;160:384-93.
30. Wadhwa, Heena, et al. "Thermal stability and dielectric relaxation behavior of in situ prepared poly (vinyl alcohol)(PVA)-reduced graphene oxide (RGO) composites." Colloid and Polymer Science 298.10 (2020): 1319-1333.
31. Balavairavan, B., S. S. Saravanakumar, and K. M. Manikandan. "Physicochemical and structural properties of green biofilms from poly (vinyl alcohol)/nano coconut shell filler." Journal of Natural Fibers (2020): 1-15.
32. Park, Gi Tae, and Jin-Hae Chang. "Comparison of Properties of PVA Nanocomposites Containing Reduced Graphene Oxide and Functionalized Graphene." Polymers 11.3 (2019): 450.
33. Zhang S, Liu P, Zhao X, Xu J. Enhanced tensile strength and initial modulus of poly (vinyl alcohol)/graphene oxide composite fibers via blending poly (vinyl alcohol) with poly (vinyl alcohol)-grafted graphene oxide. J. Polym. Research. 2018; 25(3):1-4.
34. Nandi D, Mohan VB, Bhowmick AK, Bhattacharyya D. Metal/metal oxide decorated graphene synthesis and application as supercapacitor: a review. Journal of Materials Science. 2020; 55(15):6375-400.

35. Yi CQ, Zou JP, Yang HZ, Xian LE. Recent advances in pseudocapacitor electrode materials: transition metal oxides and nitrides. Transactions of Nonferrous Metals Society of China. 2018, 1; 28(10):1980-2001.
36. Abdah MA, Azman NH, Kulandaivalu S, Sulaiman Y. Review of the use of transition-metal-oxide and conducting polymer-based fibres for high-performance supercapacitors. Materials & Design. 2020, 15;186:108199.
37. Wang Y, Chen J, Cao J, Liu Y, Zhou Y, Ouyang JH, Jia D. Graphene/carbon black hybrid film for flexible and high rate performance supercapacitor. Journal of Power Sources. 2014, 20; 271:269-77.
38. Davies A, Audette P, Farrow B, Hassan F, Chen Z, Choi JY, Yu A. Graphene-based flexible supercapacitors: pulse-electropolymerization of polypyrrole on free-standing graphene films. The Journal of Physical Chemistry C. 2011, 8;115(35):17612-20.
39. Somesh TE, Al-Gunaid MQ, Madhukar BS. Photosensitization of optical band gap modified poly(vinyl alcohol) films with hybrid AgAlO2 nanoparticles. Journal of Matls. Sci.: Materials in Electronics. 2019, 15;30(1):37-49.
40. Park, Seung-Keun, et al. "In situ hydrothermal synthesis of Mn3O4 nanoparticles on nitrogen-doped graphene as high-performance anode materials for lithium ion batteries." Electrochimica Acta 120 (2014): 452-459.
41. Iqbal, Javed, et al. "Ternary nanocomposite of cobalt oxide nanograins and silver nanoparticles grown on reduced graphene oxide conducting platform for high-performance supercapattery electrode material." Journal of Alloys and Compounds 821 (2020): 153452.
42. Deshmukh, Kalim, et al. "Highly dispersible graphene oxide reinforced polypyrrole/poly(vinyl alcohol) blend nanocomposites with high dielectric constant and low dielectric loss." RSC advances 5.76 (2015): 61933-61945.

43. Bhujel R, Rai S, Baruah K, Deka U, Biswas J, Swain BP. Capacitive and sensing responses of biomass derived silver decorated graphene. Scientific Reports. 2019, 23; 9(1):1-4.
44. Bokobza, Liliane, Jean-Luc Bruneel, and Michel Couzi. "Raman spectra of carbon-based materials (from graphite to carbon black) and of some silicone composites." C—Journal of Carbon Research 1.1 (2015): 77-94.
45. El-Gendy, Dalia M., Nabil A. Abdel Ghany, and Nageh K. Allam. "Synergistic effect of silver and adenine on boosting the supercapacitance performance of spongy graphene." Journal of Energy Storage 24 (2019): 100776.
46. Yang, Jian-He, and Yu-Der Lee. "Highly electrically conductive rGO/PVA composites with a network dispersive nanostructure." Journal of materials chemistry 22.17 (2012): 8512-8517.
47. Ishaq S, Kanwal F, Atiq S, Moussa M, Azhar U, Gul I, Losic D. Dielectric and impedance spectroscopic studies of three phase graphene/titania/poly (vinyl alcohol) nanocomposite films. Results in Physics. 2018, 1; 11:540-8.
48. Xiong P, Hu C, Fan Y, Zhang W, Zhu J, Wang X. Ternary manganese ferrite/graphene/polyaniline nanostructure with enhanced electrochemical capacitance performance. Journal of Power Sources. 2014, 15; 266:384-392.
49. Dubal DP, Holze R. All-solid-state flexible thin film supercapacitor based on Mn3O4 stacked nanosheets with gel electrolyte. Energy. 2013, 1;51:407-12.
50. Wang, Ning, et al. "Graphene–poly (vinyl alcohol) composites: Fabrication, adsorption and electrochemical properties." Applied Surface Science 314 (2014): 815-821.

51. Ishaq S, Moussa M, Kanwal F, Ehsan M, Saleem M, Van TN, Losic D. Facile synthesis of ternary graphene nanocomposites with doped metal oxide and conductive polymers as electrode materials for high performance supercapacitors. Scientific Reports. 2019, 12; 9(1):1-1.
52. Li Z, Zhou Z, Yun G, Shi K, Lv X, Yang B. High-performance solid-state supercapacitors based on graphene-ZnO hybrid nanocomposites. Nanoscale Research Letters. 2013; 8(1):1-9.
53. Sheng K, Sun Y, Li C, Yuan W, Shi G. Ultrahigh-rate supercapacitors based on electrochemically reduced graphene oxide for ac line-filtering. Scientific Reports. 2012, 3; 2(1):1-5.
54. Chandel M, Makkar P, Ghosh NN. Ag–Ni nanoparticle anchored reduced graphene oxide nanocomposite as advanced electrode material for supercapacitor application. ACS Applied Electronic Materials. 2019. 28;1(7):1215-24.
55. Theophile, Niyitanga, and Hae Kyung Jeong. "Electrochemical properties of poly (vinyl alcohol) and graphene oxide composite for supercapacitor applications." Chemical Physics Letters 669 (2017): 125-129.
56. Abdah, Muhammad Amirul Aizat Mohd, et al. "Fabrication of PEDOT coated PVA-GO nanofiber for supercapacitor." Materials Chemistry and Physics 192 (2017): 161-169.
57. Abdah MA, Rahman NA, Sulaiman Y. Enhancement of electrochemical performance based on symmetrical poly-(3, 4-ethylenedioxythiophene) coated poly(vinyl alcohol)/ graphene oxide/manganese oxide microfiber for supercapacitor. Electrochimica Acta. 2018, 1;259:466-73.

58. Arjomandi J, Lee JY, Movafagh R, Moghanni-Bavil-Olyaei H, Parvin MH. Polyaniline/aluminium and iron oxide nanocomposites supercapacitor electrodes with high specific capacitance and surface area. J. Electroanalytical Chem., 2018, 1; 810:100-8.
59. Azizi, Elmira, et al. "Fabrication of an asymmetric supercapacitor based on reduced graphene oxide/polyindole/γ− Al2O3 ternary nanocomposite with high-performance capacitive behavior." Polymer 195 (2020): 122429.
60. Bu, Ian YY, and Ray Huang. "Fabrication of CuO-decorated reduced graphene oxide nanosheets for supercapacitor applications." Ceramics International 43.1 (2017): 45-50.
61. Sinha S, Devi NA, Nongthombam S, Bhujel R, Rai S, Sarkar G, Swain BP. Investigation of optical, electrical and electrochemical properties of polyaniline/rGO/Ag2O nanocomposite. Diamond and Related Materials. 2020, 1;107:107885.
62. Islam, Muhammad Rakibul, et al. "Enhanced electrochemical performance of solution-processed single-wall carbon nanotube reinforced poly(vinyl alcohol) nanocomposite synthesized via solution-cast method." Nano Express 1.3 (2020): 030013.
63. Sharma, Bhasha, et al. "Facile synthesis of poly (vinyl alcohol) nanocomposite & its potential application to enhance electrochemical performance." Polymer Testing 74 (2019): 119-126.
64. Rose, Aleena, et al. "Electrochemical analysis of graphene oxide/polyaniline/poly(vinyl alcohol) composite nanofibers for supercapacitor applications." Applied Surface Science 449 (2018): 551-557.